A NUMERICAL INVESTIGATION TO EVALUATE THE WASHOUT OF BLOOD COMPARTMENTS IN A TOTAL ARTIFICIAL HEART

Giulia Luraghi[1], Francesco De Gaetano[1], Josè Felix Rodriguez Matas[1], Gabriele Dubini[1], Maria Laura Costantino[1], Hector De Castilla[2], Nicolas Griffaton[2], Davide Vignale[3,4], Anna Palmisano[3,4], Giuseppe Gentile[3], Antonio Esposito[3,4], Francesco Migliavacca[1].

[1]Laboratory of Biological Structure Mechanics (LaBS), Department of Chemistry, Materials and Chemical Engineering "Giulio Natta", Politecnico di Milano, Milan, Italy

[2]Carmat, Vélizy-Villacoublay, France

[3]Experimental Imaging Center, IRCCS Ospedale San Raffaele, Milan, Italy

[4]Università Vita-Salute San Raffaele, Milan, Italy

Keyword: Total Artificial Heart (TAH), Carmat, Fluid-structure Interaction (FSI), Computational Fluid-Dynamics (CFD), washout evaluation

Address for correspondence:
Francesco De Gaetano, Laboratory of
Biological Structure Mechanics (LaBS),
Department of Chemistry, Materials and
Chemical Engineering "Giulio Natta",
Politecnico di Milano, Milan, Italy.
Email: francesco.degaetano@polimi.it

ABSTRACT

Total Artificial Heart (TAH) represents the only valid alternative to heart transplantation, which number is continuously increasing in recent years. The Carmat-TAH, example of a modern generation of TAH, is a biventricular pulsatile, electrically powered, hydraulically actuated flow pump with all components embodied in a single device. One of the major issues for TAHs is the washout capability of the device, strictly correlated to the presence of blood stagnation sites. The aim of this work is to develop a numerical methodology to study the washout coupled with the fluid dynamics evaluation of the Carmat-TAH during nominal working conditions. The first part of this study, focussed on the CT scan analysis of the hybrid membrane kinematics during TAH operation which was replicated with a fluid-structure interaction simulation in the second part. The difference in percentage between the in-vitro and in-silico flow rates and stroke volume is 9.7% and 6.3%, respectively. An injection of contrast blood was simulated, and its washout was observed and quantified with the volume fraction of the contrast blood still in the ventricle. The left chamber of the device showed a superior washout performance, with a contrast volume still inside the device after four washout cycles of 6.2%, respect to the right chamber with 15%.

INTRODUCTION

The number of heart transplants and persons listed for a heart transplant is continuously increasing in recent years. From 2006 to 2018, the number of adult candidates added to the heart transplant waiting list has grown by 52% ((SRTR), 2018). Nowadays the total artificial heart (TAH) represents a valid alternative to heart transplant for patients with end-stage congestive heart failure (Cook et al., 2015). TAHs mimic the pumping action of the heart with the aim of replacing its complete function (Cohn et al., 2015; Petukhov et al., 2015). The Carmat-TAH (CARMAT SA) (Mohacsi and Leprince, 2014), developed in 1993 by the medical team of Alain Carpentier and the technical team Matra

Defense (Airbus subsidiary), is composed of two chambers, the left and the right ventricles with flexible hybrid membranes dividing the blood compartment from the driving silicon oil – the engine compartment. Two embedded electrohydraulic pumps move the oil so as to reproduce the systolic and diastolic phases of the cardiac cycle. Pumping rate and stroke volume are automatically adjusted by embedded electronic sensors and microprocessors, while the correct position of the membrane is detected by ultrasound transducers on the membranes. Preliminary clinical results with the Carmat-TAH demonstrated proper safety and hemocompatibility performance (Carpentier et al., 2015; Latrémouille et al., 2018, 2015; Smadja et al., 2017).

One of the main complications related to TAHs is the non-physiological flow patterns and stresses (Bluestein et al., 2010), causing hemolysis and thromboembolism. While blood damage is estimated from shear rate and shear stress, thromboembolism is related to the washout capability of the device (Bluestein, 2004). Washout and flow stagnation evaluation can be estimated by hydrodynamic experiments (Shettigar et al., 1989) or, increasingly, by numerical models. Computational fluid dynamic (CFD) and fluid-structure interaction (FSI) analyses are, indeed, commonly used to study Ventricular Assist Devices (VAD) and TAHs (Fraser et al., 2011).

Tambasco et al. (Tambasco and Steinman, 2002) proposed a Lagrangian approach where particles were tracked through a pre-computed 3D velocity field to evaluate a volumetric residence time on carotid arteries; the proposed methodology was later validated by 3D X-ray angiography (Ford et al., 2005) in aneurysms. Goubergrits et al. (Goubergrits et al., 2008, 2006) proposed and validated a numerical dye washout method to locate regions with high or low residence time and thrombus risk on heart valves. Prisco et al. (Prisco et al., 2017) carried out a numerical study where “virtually-dyed-blood” was washed out in a left ventricle with a VAD implantation. Similarly, Liao et al. (Liao et al., 2018b) evaluated the washout of the anatomically dilated left ventricle in the presence of inflow cannula, and the stagnation as well as the instantaneous blood volumes with low velocities and

strain rates. Sonntag et al. (Sonntag et al., 2014) quantitatively evaluated the washout performance of an existing TAH with an FSI analysis considering the interaction between the membrane and the fluids.

The aim of this work is to model the blood washout and the presence of blood stagnation sites in the Carmat-TAH during its nominal operating point conditions.

The study is organised in two steps: (i) in-vitro/in-silico comparison. The left chamber of the TAH was characterised through several experimental tests in a CT scanner by using a three-value impedance mock loop reproducing the aortic resistance, the systemic compliance and the variable systemic resistance (RCR). Subsequently, from the original CAD files, the left ventricle of the Carmat-TAH was discretised. FSI simulation reproducing the in-vitro test was carried out comparing the membrane kinematics with the experimental results. The pressures traces recorded during the experimental tests were used as boundary conditions for the in-silico comparison. (ii) Washout analysis. FSI simulations of both left and right ventricles with boundary conditions reproducing the nominal working point scenario were performed; subsequently, a CFD analysis with moving boundaries and mimicking a “contrast blood” injection and its washout was carried out.

METHODS

In-vitro test

In-vitro tests were performed at San Raffaele Hospital (Milan, Italy) with the real Carmat-TAH device working with a fixed stroke volume of 47 mL, heart rate of 60 bpm and a time ratio systole/cardiac cycle duration of 33% (parameters imposed to the rotary pump of the TAH).

An in-house three-value impedance mock loop was designed to simulate the physiological working scenario of the device (Fig. 1).

The three-value impedance mock loop, with an aortic resistance (0.9 mmHg/(L/min)) in series with the parallel circuit of a variable peripheral resistance (8 ÷ 20 mmHg/(L/min) and a compliance C

(0.141 (L/min)/(mmHg/s)) is well described in a previous paper (De Gaetano et al., 2015). Each resistance consisted of a 3D printed hollow cylinder, selecting the proper porosity in order to obtain the desired value of resistivity.

The mock loop was connected downstream of the aortic valve mimicking the aortic resistance, the systemic compliance and the variable systemic resistance (RCR).

The outlet of the RCR was connected to a free surface reservoir in order to provide a constant preload (constant inlet pressure) to the mitral valve. The right ventricle of the TAH was connected to a closed-loop since experiments were focused on the left ventricle.

The aortic flow rate was recorded by means of a transit-time ultrasonic flowmeter (HT110 series, Transonic System, Ithaca, NY, USA), while the downstream aortic pressure and upstream mitral pressure were recorded by means of pressure transducers (140 PC pressure sensors, Honeywell, NY, USA) (Fig. 1). Flow and pressure were sampled at 200 Hz using the DAQPad-6020E acquisition system (National Instruments, Inc., Austin, TX, USA). Water at T = 22°C (density ρ=1000 kg/m^3, dynamic viscosity μ=0.001 Pa·s) was used.

The images of the TAH were acquired via a Dual Source CT Scanner SOMATOM Definition Flash (Siemens Healthcare, Erlangen, Germany) with a retrospective gating including all phases of the cardiac cycle (600 mAs, 140 kV, planar resolution of 0.3671 mm x 0.3671 mm, a slice thickness of 1 mm). In order to obtain the gating, an ECG signal simulator set at the same heart rate of the artificial heart was used. The temporal resolution of the scanner was 75 ms.

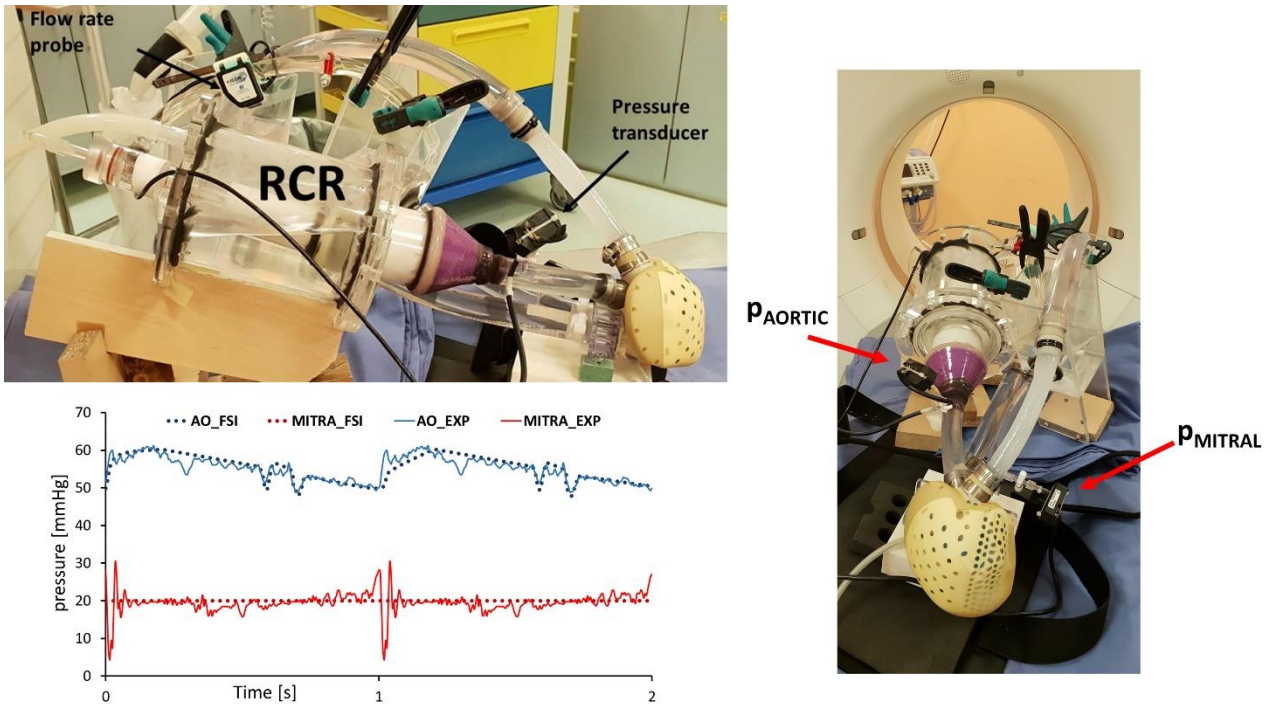

Fig. 1: (Left panel) – Carmat-TAH connected to the RCR systemic impedance simulator. Aortic and mitral pressure transducers are also shown. CT scanner was used to acquire images of the Carmat-TAH under working conditions (Right panel) – Sketch of the test bench used to reproduce and to record the pressure traces imposed as boundary conditions in the FSI simulation.

FSI analysis

The geometries of the left (red in Fig. 2a) and the right ventricle (blue in Fig. 2a) were extracted from the original CAD model provided by CARMAT SA. They consisted of the oil compartments, the flexible hybrid membranes and the blood compartments. The ventricle walls were considered as rigid structures, and they were meshed with 28,718 and 32,853 quadrangular elements for the left and the right ventricles, respectively. The geometry, and consequently the mesh, of the membranes and the valves were the same for the right and the left ventricles (Fig. 2b-c). The Carmat's membranes, which are composed of two different layers: 0.4 mm of polyurethane on the oil side, and 0.4 mm of bovine pericardium on the blood side, were discretized with 64,208 fully integrated solid elements of 0.1 mm length and of high quality (hexahedral mapped meshing with aspect ratio

and Determinant close to 1), with a total of 8 elements through-thickness. The walls and the membrane were connected node by node to prevent any leakage of fluid and any artificial contact between the membrane and the walls. The mitral and aortic valves in the left ventricle, and the tricuspid and pulmonary valves in the right ventricle, were 16-mm height and 25 mm of diameter tri-leaflets pericardium valves. Each valve was discretized with 1,806 quadrangular reduced integration with viscous hourglass shell elements with 0.32 mm of thickness and connected node by node to the walls. A sensitivity analysis of the damping coefficient for each deformable part was performed in order to smooth out the oscillations of the structure (Luraghi et al., 2018a). The properties assigned to the different model parts are listed in a previous work of ours (Luraghi et al., 2018b).

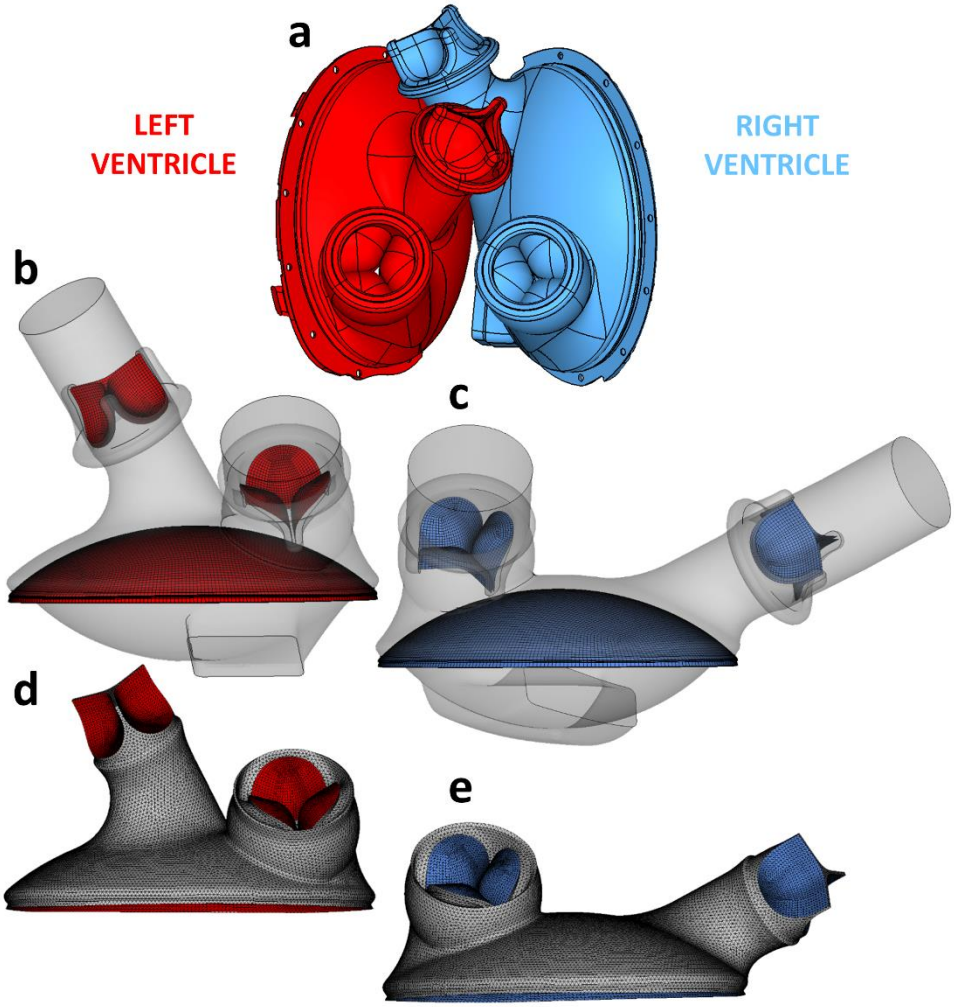

Fig. 2: (a) CAD model of the Carmat-Total Artificial Heart (TAH) with assembled left (in red) and right (in blue) ventricles, (b-c) left and right ventricle rigid walls with the discretized membrane and valves for the FSI analysis, (d-e) meshes of the left and right blood domain for the CFD analysis.

The fluid domains consisted of four components: the main volume, the oil velocity inlet, the mitral (or tricuspid) pressure inlet and the aortic (or pulmonary) pressure inlet. They were discretized with 443,134 and 503,084 Eulerian high-quality (hexahedral mapped meshing with aspect ratio and determinant close to 1) multi-material elements for the left and the right ventricles, respectively. All meshes were built with Hypermesh (Altair Eng. Inc., Troy, MI, USA).

The structures were all immersed into the fluid domain, as the "operator split" algorithm (Benson, 1992) which was implemented in the finite element solver LS-DYNA 971 Release 10.0 (LSTC, Livermore, CA, USA) was used to couple the fluid and the structure domains. More technical details regarding the FSI methodology can be found in previous studies of ours (Luraghi et al., 2019, 2017; Wu et al., 2016).

As per the in-vitro/FSI comparison analysis on the left ventricle, the imposed flow rate (dashed curve in Fig. 3) on the oil inlet was the same imposed by the rotary pump (fix stroke volume of 47 mL, frequency of 60 bpm and time ratio systole/cycle of 33%), whereas the filtered pressure traces registered during the in-vitro test were applied on the mitral inlet and the aortic outlet. For this FSI model, the physical properties of water (density ρ=1000 kg/m^3 and dynamic viscosity μ=0.001 Pa·s) were used to model the fluid in the blood compartment.

As per the numerical washout analysis, the nominal working point scenario for both the left and the right ventricles were modelled by imposing a flow rate curve (continuous curve in Fig. 3) with a fix stroke volume of 60 mL, frequency of 90 bpm and time ratio systole/cycle of 35%. Zero pressure condition was applied on both the mitral and tricuspid inlets, while 120 mmHg and 35 mmHg were

applied on the aortic and pulmonary outlet, respectively. In this case, the physical properties of the blood (density ρ=1060 kg/m^3 and dynamic viscosity μ=0.00356 Pa·s) were used for the fluid in the blood compartment.

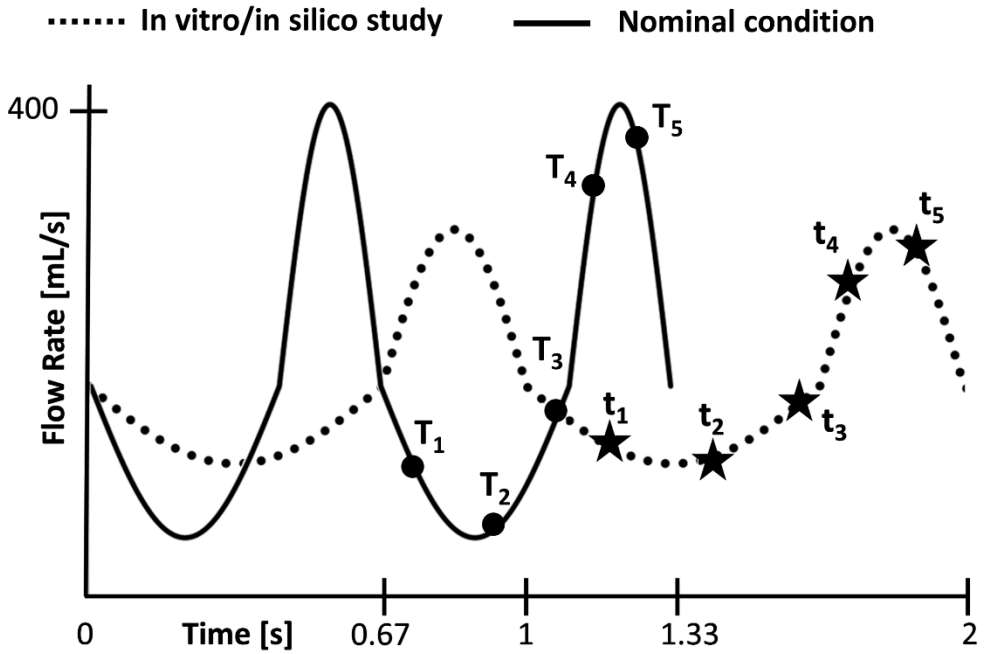

Fig. 3: Imposed oil flow rates in the FSI models reproducing the experimental tests (dotted line) used for the in-vitro/in-silico comparison and the nominal working condition (continuous line) imposed for the washout analysis. The stars and the dots on the curves indicate the time-points where results are shown.

CFD and Washout analysis

The finite volume solver Fluent 18.0 (ANSYS Inc., Canonsburg, PA, USA) was used to discretize the blood domains with the *Meshing Mode* tool, and to solve the hemodynamics coupled with the washout analysis. The movement of the membranes and the valves from the FSI analysis were imposed at the fluid grid by means of a user-defined function implemented in the Dynamic Mesh algorithm. Meshes were deformed both through smoothing and remeshing methods: the former with a diffusion algorithm with a diffusion parameter of 2, the latter with a combination of local face

and region face algorithms performed at each time-step. The time integration was performed using a second-order implicit scheme, while the space integration was performed using a second-order upwind scheme. The constant time-step chosen in the CFD simulations was the same we used to export the results from the FSI analysis.

The washout evaluation was performed by means of the volume of fluid (VOF) approach, as suggested by Sonntag et al. (Sonntag et al., 2014). VOF is a Eulerian-Eulerian approach to track the interface of two immiscible fluids, blood (phase 1) and contrast blood (phase 2). Blood and contrast blood were set with the same Newtonian fluid properties defined in the FSI simulations (density ρ=1060 kg/m^3 and dynamic viscosity μ=0.00356 Pa·s).

The volume fractions of the blood (phase 1) and contrast blood (phase 2) are defined as:

$$\alpha_1 = \frac{\delta V_1}{\delta V}, \quad (1)$$

$$\alpha_2 = \frac{\delta V_2}{\delta V}, \quad (2)$$

where V_1, V_2 and V are the volumes of phase 1, phase 2, and of the total blood domain, respectively. By definition, $V_1 + V_2 = V$ so, consequently, the sum of α_1 and α_2 must be one. A single momentum equation was solved for the mixture of all fluids, and the resulting velocity field was shared between the phases. Based on the local values of α_1 and α_2, the appropriate properties and variables were assigned to each control volume within the domain. The interface between the phases was tracked by solving the volume fraction continuity equation of each phase:

$$\frac{\partial(\alpha_1\rho_1)}{\partial t} + \nabla \cdot (\alpha_1\rho_1\boldsymbol{u}) = 0, \quad (3)$$

$$\frac{\partial(\alpha_2\rho_2)}{\partial t} + \nabla \cdot (\alpha_2\rho_2\boldsymbol{u}) = 0, \quad (4)$$

where ρ_1 and ρ_2 are the densities of phase 1 and phase 2, respectively, and $\boldsymbol{u}$ is the mixture velocity. VOF was solved by means of an implicit time discretization, where the phase continuity equation (3) was solved iteratively together with velocities and pressures (ANSYS, 2018).

After two cycles of initialization with blood (phase 1), where all the cells displayed a α_1 value of 1 (*cycles I* and *II* in Figs. 6-7), an injection of contrast blood (phase 2) was simulated by setting α_2 equal to 1 at the mitral or tricuspid pressure inlets (*cycle III* in Figs. 6-7). After *cycle III*, four washout cycles, where blood (phase 1, $\alpha_1 = 1$) re-entered the ventricle, were performed (*cycles IV, V, VI* and *VII* in Figs. 6-7). The volume fractions of the contrast blood (phase 2, α_2) was set equal zero in both aortic and pulmonary outlet to avoid contrast blood backflow from the outlets.

Following the same methodology published by Luraghi and colleagues (Luraghi et al., 2018b), the blood compartments of the left and the right ventricles were isolated and discretized with 199,975 and 205,465 tetrahedral elements respectively (Fig. 2d-e) based on a mesh sensitivity analysis summarized in Table 1. In particular, the VOF algorithm resulted sensitive to the mesh size. The selected grid (grid #2 in Table 1) displayed a difference of less than 4%, in the parameter α_2 with respect to the finer grid (grid #3 in Table 1), during the first 5 time-steps of *cycle III*. Hence, for the left ventricle, tetrahedral cells of 0.5 mm average element-size looked more appropriate. The same criteria were adopted for the right ventricle.

Table 1: different grids (from #1 to #3 with the corresponding numbers of total elements) considered for the mesh sensitivity analysis and the resulted convergence variable, the values of α_2 (2) after 5 time-steps.

Grid (Left ventricle)	Total elements	α_2 (2) after 5 time-steps
#1	109,362	0.02474

#2	199,675	0.02749
#3	319,234	0.02859

RESULTS

In-vitro/FSI comparison

The kinematics of the membrane of the left ventricles acquired with the CT scan was overlapped with that obtained from the FSI simulation. Indeed, the 2D images were segmented to reconstruct the membrane profile and its movement during the working cycle. In this regard, the CT acquisitions resulted profoundly affected by the presence of metallic artefacts, especially from the engine parts. The cross-section shown in Fig. 4 is the only section of the device where the membrane profile was clearly identified.

Starting from its initial position (t_1), the oil fluid dynamics governed by the electrohydraulic pump determined an inversion of the membrane curvature that completely unfurled during the diastolic phase (t_2-t_3). During the systolic phase (t_4- t_5), the membrane reverted to its initial configuration, by ejecting the stroke volume of fluid through the open aortic valve. The membrane position calculated in the FSI simulation of the left ventricle was used for the comparison. The same section of the CT plane acquisition was examined and the membrane profiles from the model were overlapped in the images.

In addition, a quantitative comparison was performed with the hemodynamic parameters registered during the experiment. The mean volume flow rate from the FSI simulation was 2.57 L/min, while that measured from the in-vitro test was 2.32 L/min, resulting in an underestimation of 9.7%. The stroke volume from the FSI simulation was 42.8 mL, a 6.3% lower than the stroke volume (47 mL) set on the rotary pump.

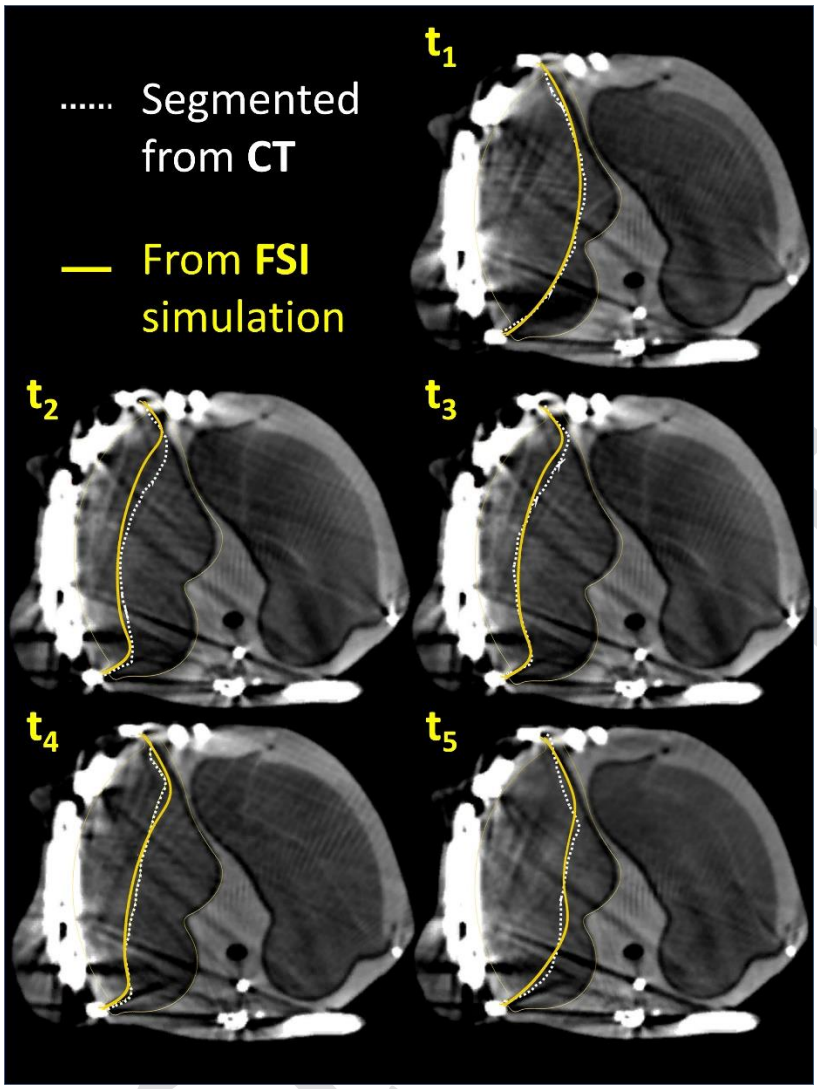

Fig. 4: Comparison between the membrane profiles of the left ventricle segmented from the CT acquisition (white dashed lines) and the profiles resulting from the FSI simulations (continuous yellow lines) at different time points along the cardiac cycle (black stars in Fig. 3).

Washout analysis

FSI simulations of the left and right ventricles to mimic the nominal scenario were performed, and the resulting movement of the membrane and valves leaflets were exported and used as moving boundaries in the CFD simulation.

Velocity patterns from the CFD analysis both for the left and the right ventricles are shown in Fig. 5 at five different time-steps during the cardiac cycle, from the diastole (T_1, T_2 and T_3) to the systole (T_4 and T_5).

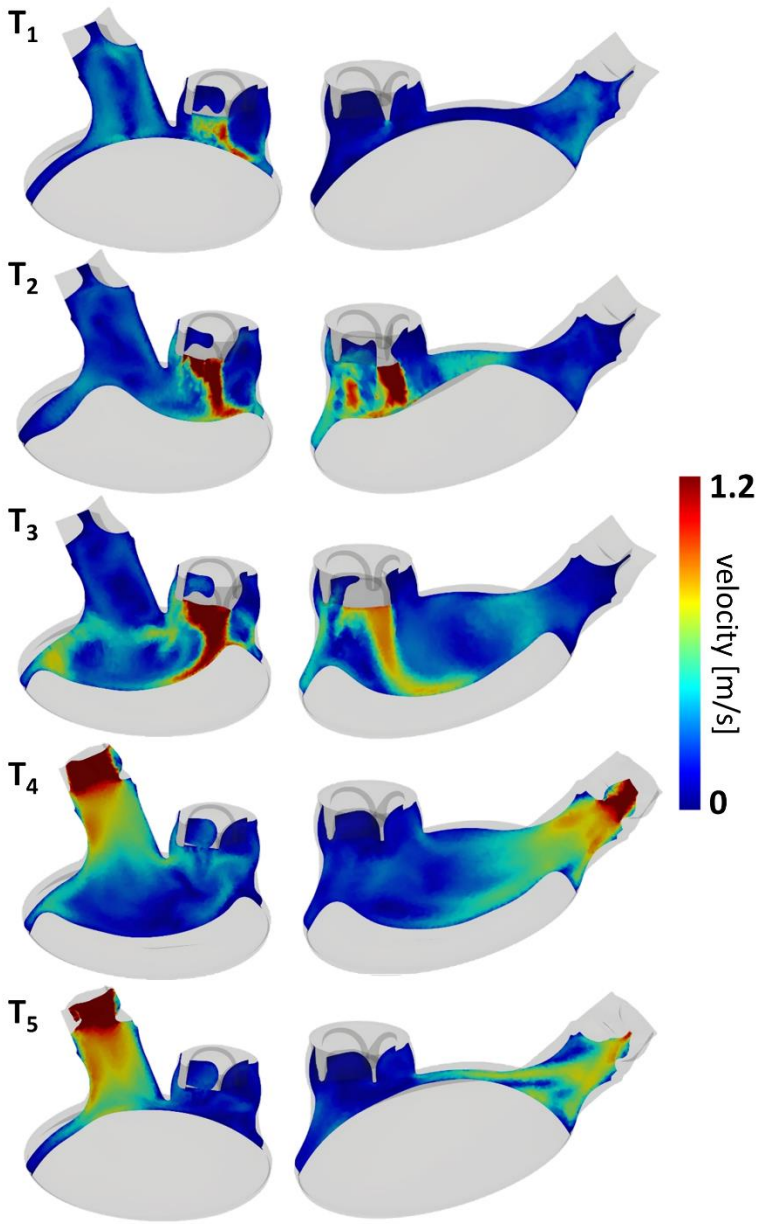

Fig. 5: Velocity patterns from the CFD simulations for both the left (left panel) and right (right panel) ventricles at different instants along the cardiac cycle (black points in Fig.3). The membrane and valves displacements calculated by the FSI simulations are clearly visible.

At the beginning of the diastolic phase (T_1), the mitral valve in the left ventricle opened faster than the tricuspid valve in the right ventricle. However, at the full inlet valves opening the maximum blood velocity resulted similar (1.74 m/s for the left ventricle and 1.77 m/s for the right ventricle at T_2). The timing to evolve from diastole to systole for the ventricles was not identical, as observed at

T_3, due to the different membrane displacement and pressure conditions that the ventricles were subjected to. The maximum velocity in systole and the peak timings were different for the ventricles, 2.09 m/s at T_5 for the left ventricle, while 1.73 m/s at T_4 for the right ventricle. The evolution of the velocity patterns during the cardiac cycle is determinant to understand the washout analysis. Moreover, velocity fields resulted repeatable in all the simulated cycles, two of initialization (*cycles I* and *II* in Figs. 6-7), one of contrast blood injection (*cycle III* in Figs. 6-7) and four of washout (*cycles IV, V, VI* and *VII* in Figs. 6-7).

The visualization of the location of contrast blood inside the ventricles during the injection and during the washout cycles is a crucial aspect to study the washout capability of the TAH. Figure 6 and Figure 7 illustrate the presence of blood (phase 1 – grey-coloured) and contrast blood (phase 2 – red-coloured) in one section of the device. During the injection cycle (*cycle III*), the contrast blood was constrained to enter through the mitral -or tricuspid- valve in the ventricles and to mix with the blood in the ventricles. The contrast blood position in this cycle (*cycle III*) reflects the contour of the magnitude of the velocity since the largest presence of contrast blood was located at the points where the velocity was higher. During the systole of the injection cycle, the first blood to exit thought the aortic or pulmonary valve was the blood of phase 1, followed by the contrast one.

Conversely, during the following washout cycles, the entering blood of phase 1 followed the velocity contours, while the remaining contrast blood was confined to low-velocity zones or to fluid recirculation areas where the blood failed to leave.

For the sake of clarity, the quantification of the fraction of contrast blood α_2 (Eq. 2) did not consider the change of the ventricular volumes over time, but the total blood of the domain in the denominator was kept constant and equal to the initial volume of the ventricle.

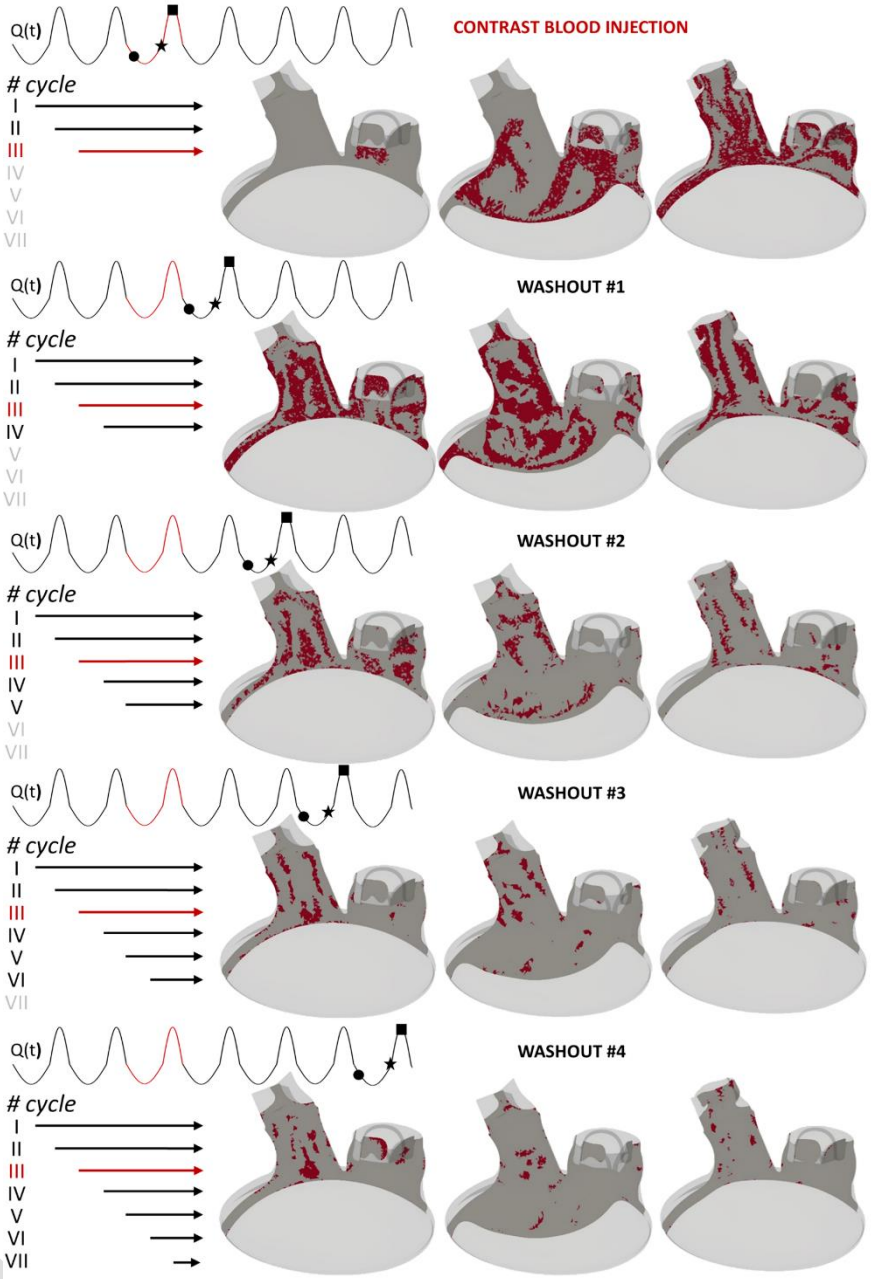

Fig. 6: Washout evaluation for the left ventricle at different dots during the contrast blood injection cycle (*cycle III*) and during the following washout cycles (*cycles IV, V, VI* and *VII*). The contrast blood (phase 2) is coloured in red, while the blood (phase 1) in grey. The coloured arrows next the cycle numbers indicate the blood phase entering in the shown cycle. Circle, star, and squared markers on the flow rate waveform refer respectively to the first, second and third images from the left for each washout evaluation.

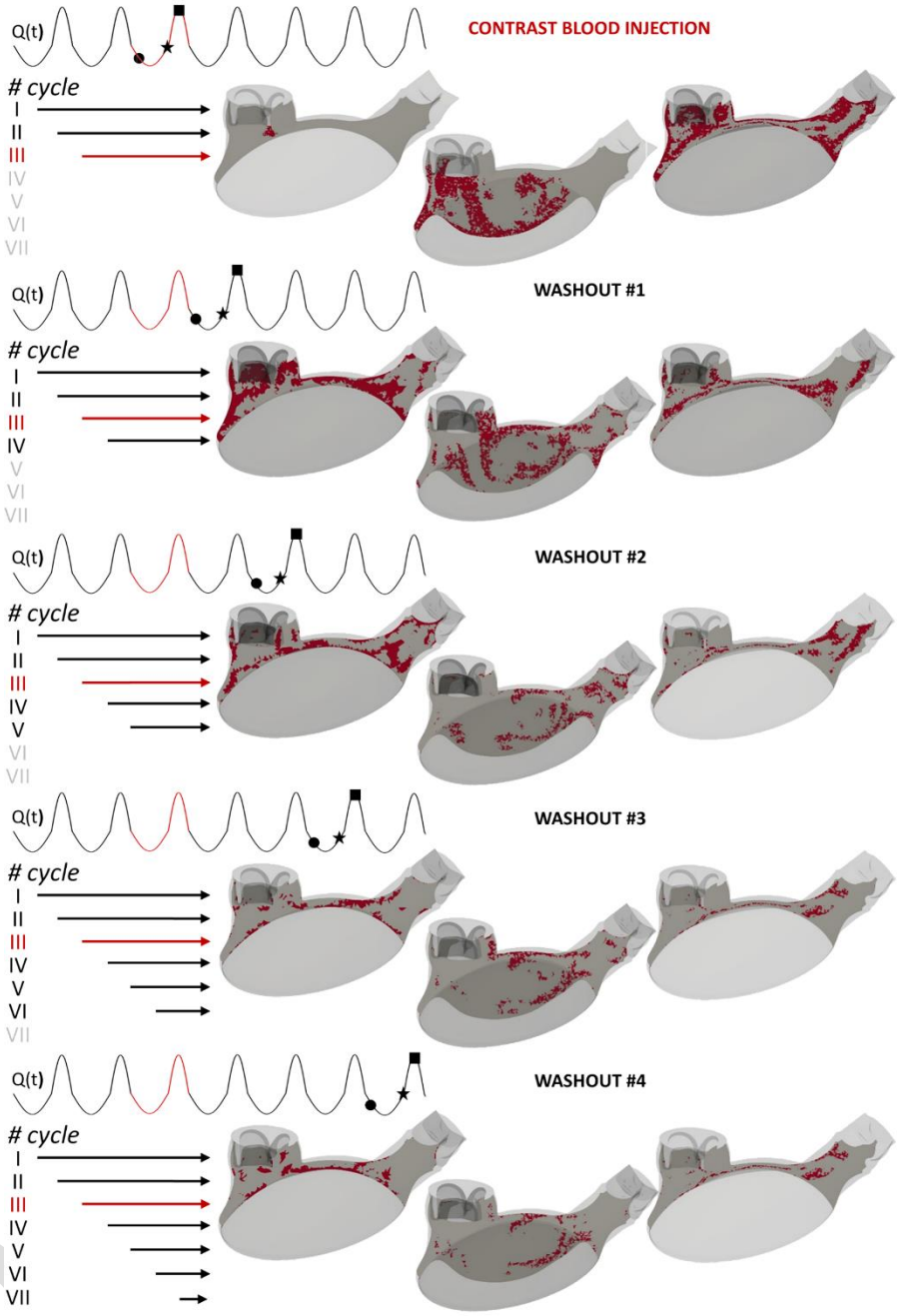

Fig. 7: Washout evaluation for the right ventricle at different dots during the contrast blood injection cycle (*cycle III*) and during the following washout cycles (*cycles IV, V, VI* and *VII*). The contrast blood (phase 2) is coloured in red, while the blood (phase 1) in grey.

At the end of the contrast injection cycle (*cycle III*) the volume fraction of contrast blood (phase 2) still inside the ventricles resulted in 61 % and in 53 % of the total volume for the left and the right ventricle respectively. At the end of the washout cycles the volume fraction of phase 2 resulted in

29% (*cycle IV*), 14% (*cycle V*), 8.5% (*cycle VI*) and 6.2% (*cycle VII*) for the left ventricle and in 37% (*cycle IV*), 24% (*cycle V*), 18% (*cycle VI*) and 15% (*cycle VII*) for the right ventricle (Fig. 8c-d) and possible contrast blood stagnation areas were identified (Fig. 8a-b). More precisely, in both the ventricles after the last washout cycle *(cycle VII)* the contrast blood stagnated at the wall -in the narrow edges- and in the proximity of the valves' locations.

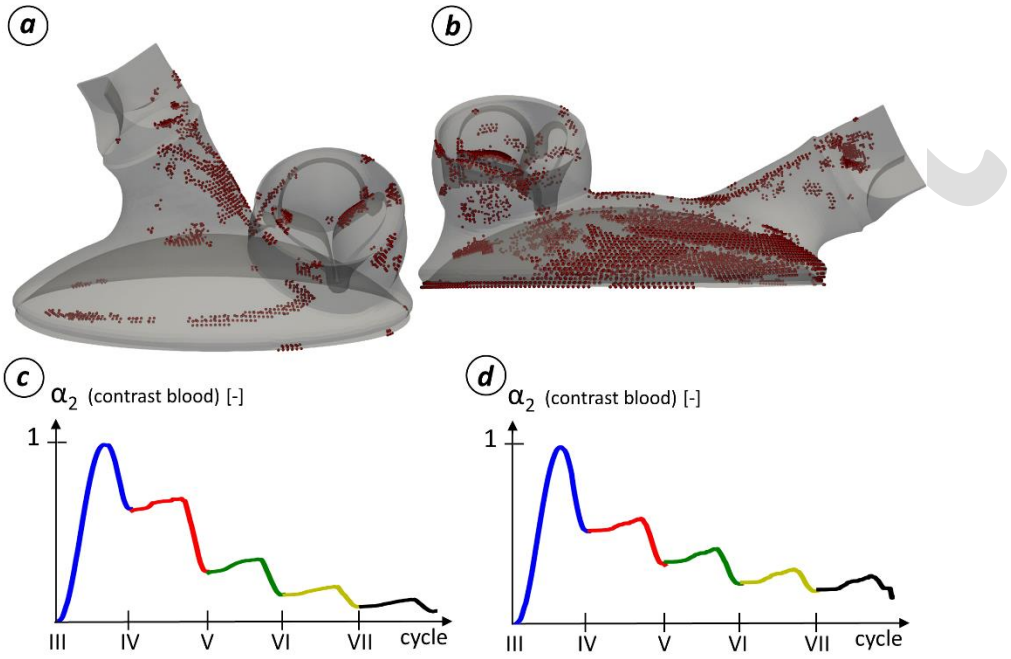

Fig. 8: (a-b) Contrast blood after the last washout cycle *(cycle VII)* for the left and right ventricles; (c-d) temporal volumetric fraction of contrast blood curve from the injection for the left and right ventricles. In the equation of α_2 (Eq. 2) the total blood of the domain at the denominator was kept constant and equal to the initial volume of the ventricle.

DISCUSSION

TAHs represent the only effective long-term treatment for patients with advanced bi-ventricular heart failure, as an alternative to heart transplantation. Haemolysis and thromboembolism are the main dangerous complications of these devices. The former is related to blood damage, the latter to the washout capability of the device (Bluestein et al., 2010). In this study, a numerical

methodology to evaluate the washout and the presence of blood stagnation sites in the Carmat-TAH was proposed. A numerical workflow to reproduce the hemodynamics inside the left ventricle of the Carmat-TAH together with the movement of the valves and the membrane was already presented (Luraghi et al., 2018b). It was the first work where a CFD analysis of a TAH considered the realistic kinematics of the valves and the membrane from a fully coupled and 2-ways FSI analysis.

The first part of this work consisted of the comparison of the published methodology with the experimental tests. In particular, a CT scanner acquired the left chamber of the TAH during its operation. An excellent quantitative comparison of the hemodynamic parameters was achieved with errors in the volume flow rate and volume stroke lower than 10% and 7% respectively. A segmentation process on the acquired 2D images was performed to reconstruct the membrane profile. Its comparison with the membrane profile from the FSI simulation, in the same plane, was acceptable. It is known, indeed, that the membrane motion in TAHs is considered the most critical part of the device performance and thus accurate modelling would be required (Long et al., 2013).

The second part of this work was aimed at including the evaluation of the washout in the CFD analysis. In the literature, different washout evaluation methods were proposed, *e.g.* by means of experimental analysis (Shettigar et al., 1989), Lagrangian-based (Ford et al., 2005; Tambasco and Steinman, 2002) or Eulerian-based (Goubergrits et al., 2008, 2006; Liao et al., 2018a; Prisco et al., 2017; Sonntag et al., 2014) numerical algorithms. We proposed a VOF algorithm to model a contrast blood injection into the ventricles and its disappearance was observed. Although the same methodology was already adopted to study the washout of an existing TAH, but neglecting the valve opening and closing phases (Sonntag et al., 2014), to the best of our knowledge this is the first CFD study with moving boundaries to consider the kinematics of the membrane and of both the inlet and outlet valves coupled with a VOF algorithm, The modelling of the valves kinematics is imperative to be included in the CFD analysis of TAHs since the fluid dynamics in the absence of valves differs

in terms of global and local velocity fields (Luraghi et al., 2018b). After two cycles for the fluid initialization, contrast blood was injected into the ventricles, followed by four washout cycles. The volume fractions of the contrast blood still inside the ventricle domain gave indication about the washout performance of the device and possible stagnation areas. Results indicate that complete blood washout is not fully achieved over the four cardiac cycles with about 6% and 15% of the blood remaining within the two ventricles. The washout of the left ventricle is estimated more efficient if compared to the one of the right ventricle, due to the different geometric features of the chambers.

Limitations

This study showed, however, some limitations. Unfortunately, as already observed in the literature (Sonntag et al., 2013), a detailed quantitative comparison between in-vitro analysis and numerical test is limited due to the restricted field of view of the membrane in the experimental set-up. A complete 3D segmentation of the membrane from CT images was not possible due to the massive metallic artefacts of the CT acquisitions, mainly due to the engine parts. There is only one available cross-section where the membrane profile was clearly identified and segmented.

Secondly, the boundary conditions prescribed to the ventricles in the washout analysis wanted to replicate the nominal working conditions of the device but, in the future, a lumped parameter model could be integrated. The fluid flow was considered with a laminar model, but the use of different turbulent models, such as the Reynolds Averaged Navier Stokes or Large Eddy Simulations, could be investigated. A proper validation on the fluid flow, has still to be considered but the complex geometry with metallic parts of the real Carmat-TAH prevents from using Magnetic Resonance Imaging and makes the Particle Image Velocimetry technique hard to use.

CONCLUSION

The adopted numerical workflow composed of sequential simulations, a 2-way fully-coupled FSI analysis and a CFD with VOF algorithm analysis, can give an accurate prediction of the washout

capability of the device and allows visualizing the blood stagnation areas. The membrane kinematics resulted from the FSI analysis and used to dynamically move the grid in the CFD analysis was also verified experimentally. This in-silico methodology can help designing and optimizing a device able to reduce the potential thromboembolism for patients with TAH.

REFERENCES

(SRTR), O.P. and T.N. (OPTN) and S.R. of T.R., 2018. Organ Procurement and Transplantation Network (OPTN) and Scientific Registry of Transplant Recipients(SRTR). OPTN/SRTR 2017 Annual Data Report. [WWW Document]. Rockville,MD Dep. Heal. Hum. Serv. Heal. Resour. Serv. Adm. Healthc. Syst. Bur. Div. Transplant.

ANSYS, I., 2018. ANSYS Fluent Theory Guide.

Benson, D.J., 1992. Computational methods in Lagrangian and Eulerian hydrocodes. Comput. Methods Appl. Mech. Eng. 99, 235–394. https://doi.org/10.1016/0045-7825(92)90042-I

Bluestein, D., 2004. Research approaches for studying flow-induced thromboembolic complications in blood recirculating devices. Expert Rev. Med. Devices 1, 65–80. https://doi.org/10.1586/17434440.1.1.65

Bluestein, D., Chandran, K.B., Manning, K.B., 2010. Towards non-thrombogenic performance of blood recirculating devices. Ann. Biomed. Eng. 38, 1236–56. https://doi.org/10.1007/s10439-010-9905-9

Carpentier, A., Latrémouille, C., Cholley, B., Smadja, D.M., Roussel, J.C., Boissier, E., Trochu, J.N., Gueffet, J.P., Treillot, M., Bizouarn, P., Méléard, D., Boughenou, M.F., Ponzio, O., Grimmé, M., Capel, A., Jansen, P., Hagège, A., Desnos, M., Fabiani, J.N., Duveau, D., 2015. First clinical use of a bioprosthetic total artificial heart: Report of two cases. Lancet 386, 1556–1563. https://doi.org/10.1016/S0140-6736(15)60511-6

Cohn, W.E., Timms, D.L., Frazier, O.H., 2015. Total artificial hearts: past, present and future. Nat.

Rev. Cardiol. 12, 609–617. https://doi.org/10.1038/nrcardio.2015.79

Cook, J.A., Shah, K.B., Quader, M.A., Cooke, R.H., Kasirajan, V., Rao, K.K., Smallfield, M.C., Tchoukina, I., Tang, D.G., 2015. The total artificial heart. J. Thorac. Dis. 7, 2172–80. https://doi.org/10.3978/j.issn.2072-1439.2015.10.70

De Gaetano, F, Serrani, M, Bagnoli, P, Brubert, J, Stasiak, J, Moggridge, G.D, Costantino, M.L., 2015. Fluid dynamic characterization of a polymeric heart valve prototype (Poli-Valve) tested under continuous and pulsatile flow conditions. Int J Artif Organs 2015; 38(11): 600-606. https://doi.org/ 10.5301/ijao.5000452

Ford, M.D., Stuhne, G.R., Nikolov, H.N., Habets, D.F., Lownie, S.P., Holdsworth, D.W., Steinman, D.A., 2005. Virtual angiography for visualization and validation of computational models of aneurysm hemodynamics. IEEE Trans. Med. Imaging 24, 1586–1592. https://doi.org/10.1109/TMI.2005.859204

Fraser, K.H., Taskin, M.E., Griffith, B.P., Wu, Z.J., 2011. The use of computational fluid dynamics in the development of ventricular assist devices. Med. Eng. Phys. 33, 263–280. https://doi.org/10.1016/j.medengphy.2010.10.014

Goubergrits, L., Kertzscher, U., Affeld, K., Petz, C., Stalling, D., Hege, H.-C., 2008. Numerical Dye Washout Method as a Tool for Characterizing the Heart Valve Flow: Study of Three Standard Mechanical Heart Valves. ASAIO J. 54, 50–57. https://doi.org/10.1097/MAT.0b013e31815c5e38

Goubergrits, L., Timmel, T., Affeld, K., Petz, C., Stalling, D., Hege, H.C., 2006. Characterization of an Artificial Valve Flow Using the Numerical Dye Washout Visualization Technique: Application to the Monoleaflet Valve With Purged Flow. Artif. Organs 30, 642–650. https://doi.org/10.1111/j.1525-1594.2006.00277.x

Latrémouille, C., Carpentier, A., Leprince, P., Roussel, J.-C., Cholley, B., Boissier, E., Epailly, E.,

Capel, A., Jansen, P., Smadja, D.M., 2018. A bioprosthetic total artificial heart for end-stage heart failure: Results from a pilot study. J. Hear. Lung Transplant. 37, 33–37. https://doi.org/10.1016/j.healun.2017.09.002

Latrémouille, C., Duveau, D., Cholley, B., Zilberstein, L., Belbis, G., Boughenou, M.-F., Meleard, D., Bruneval, P., Adam, C., Neuschwander, A., Perles, J.-C., Jansen, P., Carpentier, A., 2015. Animal studies with the Carmat bioprosthetic total artificial heart. Eur. J. Cardio-Thoracic Surg. 47, e172–e179. https://doi.org/10.1093/ejcts/ezv010

Liao, S., Neidlin, M., Li, Z., Simpson, B., Gregory, S.D., 2018a. Ventricular flow dynamics with varying LVAD inflow cannula lengths: In-silico evaluation in a multiscale model. J. Biomech. 72, 106–115. https://doi.org/10.1016/j.jbiomech.2018.02.038

Liao, S., Wu, E.L., Neidlin, M., Li, Z., Simpson, B., Gregory, S.D., 2018b. The Influence of Rotary Blood Pump Speed Modulation on the Risk of Intraventricular Thrombosis. Artif. Organs 42, 943–953. https://doi.org/10.1111/aor.13330

Long, C.C., Marsden, A.L., Bazilevs, Y., 2013. Fluid-structure interaction simulation of pulsatile ventricular assist devices. Comput. Mech. 52, 971–981. https://doi.org/10.1007/s00466-013-0858-3

Luraghi, G., Migliavacca, F., García-González, A., Chiastra, C., Rossi, A., Cao, D., Stefanini, G., Rodriguez Matas, J.F., 2019. On the Modeling of Patient-Specific Transcatheter Aortic Valve Replacement: A Fluid-Structure Interaction Approach. Cardiovasc. Eng. Technol. 10, 437–455. https://doi.org/10.1007/s13239-019-00427-0

Luraghi, G., Migliavacca, F., Rodriguez Matas, J.F., 2018a. Study on the Accuracy of Structural and FSI Heart Valves Simulations. Cardiovasc. Eng. Technol. 9, 1–16. https://doi.org/10.1007/s13239-018-00373-3

Luraghi, G., Wu, W., De Castilla, H., Rodriguez Matas, J.F., Dubini, G., Dubuis, P., Grimmé, M.,

Migliavacca, F., 2018b. Numerical Approach to Study the Behavior of an Artificial Ventricle: Fluid-Structure Interaction Followed By Fluid Dynamics With Moving Boundaries. Artif. Organs 42, E315–E324. https://doi.org/10.1111/aor.13316

Luraghi, G., Wu, W., De Gaetano, F., Rodriguez Matas, J.F., Moggridge, G.D., Serrani, M., Stasiak, J., Costantino, M.L., Migliavacca, F., 2017. Evaluation of an aortic valve prosthesis: Fluid-structure interaction or structural simulation? J. Biomech. 58, 45–51. https://doi.org/10.1016/j.jbiomech.2017.04.004

Mohacsi, P., Leprince, P., 2014. The CARMAT total artificial heart. Eur. J. Cardio-Thoracic Surg. 46, 933–934. https://doi.org/10.1093/ejcts/ezu333

Morgan, J.A., Brewer, R.J., Nemeh, H.W., Gerlach, B., Lanfear, D.E., Williams, C.T., Paone, G., 2014. Stroke While on Long-Term Left Ventricular Assist Device Support. ASAIO J. 60, 284–289. https://doi.org/10.1097/MAT.0000000000000074

Petukhov, D.S., Selishchev, S. V., Telyshev, D. V., 2015. Total Artificial Heart: State-of-the-art. Biomed. Eng. (NY). 49, 193–196. https://doi.org/10.1007/s10527-015-9528-4

Prisco, A.R., Aliseda, A., Beckman, J.A., Mokadam, N.A., Mahr, C., Garcia, G.J.M., 2017. Impact of LVAD Implantation Site on Ventricular Blood Stagnation. ASAIO J. 63, 392–400. https://doi.org/10.1097/MAT.0000000000000503

Shettigar, U.R., Dropmann, M., Christian, P.E., Kolff, W.J., 1989. Residence time distributions in artificial ventricles. ASAIO Trans. 35, 708–12.

Smadja, D.M., Susen, S., Rauch, A., Cholley, B., Latrémouille, C., Duveau, D., Zilberstein, L., Méléard, D., Boughenou, M.-F., Belle, E. Van, Gaussem, P., Capel, A., Jansen, P., Carpentier, A., 2017. The Carmat Bioprosthetic Total Artificial Heart Is Associated With Early Hemostatic Recovery and no Acquired von Willebrand Syndrome in Calves. J. Cardiothorac. Vasc. Anesth. 31, 1595–1602. https://doi.org/10.1053/J.JVCA.2017.02.184

Sonntag, S.J., Kaufmann, T.A.S., Büsen, M.R., Laumen, M., Gräf, F., Linde, T., Steinseifer, U., 2014. Numerical washout study of a pulsatile total artificial heart. Int. J. Artif. Organs 37, 241–252. https://doi.org/10.5301/ijao.5000306

Sonntag, S.J., Kaufmann, T.A.S., Büsen, M.R., Laumen, M., Linde, T., Schmitz-Rode, T., Steinseifer, U., 2013. Simulation of a pulsatile total artificial heart: Development of a partitioned Fluid Structure Interaction model. J. Fluids Struct. 38, 187–204. https://doi.org/10.1016/J.JFLUIDSTRUCTS.2012.11.011

Tambasco, M., Steinman, D.A., 2002. On Assessing the Quality of Particle Tracking Through Computational Fluid Dynamic Models. J. Biomech. Eng. 124, 166. https://doi.org/10.1115/1.1449489

Wu, W., Pott, D., Mazza, B., Sironi, T., Dordoni, E., Chiastra, C., Petrini, L., Pennati, G., Dubini, G., Steinseifer, U., Sonntag, S., Kuetting, M., Migliavacca, F., 2016. Fluid–Structure Interaction Model of a Percutaneous Aortic Valve: Comparison with an In Vitro Test and Feasibility Study in a Patient-Specific Case. Ann. Biomed. Eng. 44, 590–603. https://doi.org/10.1007/s10439-015-1429-x